



## Understanding the asymmetry between advancing and receding microscopic contact angles

Journal:	<i>Soft Matter</i>
Manuscript ID	SM-ART-03-2019-000521.R1
Article Type:	Paper
Date Submitted by the Author:	08-Apr-2019
Complete List of Authors:	Omori, Takeshi; Osaka University, Mechanical Engineering Kobayashi, Yosuke; Osaka University, Mechanical Engineering Yamaguchi, Yasutaka; Osaka University, Department of Mechanical Engineering Kajishima, Takeo; Osaka University, Mechanical Engineering

Cite this: DOI: 00.0000/xxxxxxxxxx

## Understanding the asymmetry between advancing and receding microscopic contact angles

T. Omori,<sup>\*a</sup> Y. Kobayashi,<sup>a</sup> Y. Yamaguchi<sup>a</sup> and T. Kajishima<sup>a</sup>Received Date  
Accepted Date

DOI: 00.0000/xxxxxxxxxx

By means of molecular dynamics simulation, the advancing and receding microscopic contact angles were analyzed for a shear flow of two mono-atomic fluids confined between parallel non-polar solid walls. We defined the microscopic dynamic contact angle based on the coarse-grained microscopic density distribution of the fluids (the instantaneous interface method [Willard and Chandler, *J. Phys. Chem. B* **114**, 1954–1958 (2010)]) near the moving contact line. We have found that the asymmetric change of fluid density near the wall with respect to the moving contact line results in a different dependence between the advancing and receding contact angles on the contact line velocity in a system where the two fluids across the interface have unequal wettability to the solid wall. This difference between the advancing and receding contact angles leads to different flow resistance caused by the advancing and receding contact lines, which should have impact on the industrial applications of the fine fluid transportation with contact lines.

### 1 Introduction

The prediction of dynamic wetting is of significant theoretical and practical interest, and measuring and modeling of dynamic contact angles (CAs) have been an active subject of research over the last decades<sup>1,2</sup>. One of the fundamental problems toward the modeling of dynamic CAs is the possible arbitrariness in its definition. They may be totally different depending on which part of the fluid interface is considered to form an angle to the solid surface. In particular, there is even a qualitative difference between the microscopic dynamic CA measured in the molecular vicinity of the contact line (CL) and the macroscopic dynamic CA measured elsewhere<sup>3–5</sup>.

In terms of predicting the flow with CLs, it has been demonstrated<sup>6</sup> that the microscopic dynamic CA is a more fundamental quantity than the macroscopic dynamic CA and is a more suitable quantity to be implemented in the boundary condition for the fluid momentum equation (see also Qian *et al.*<sup>7</sup>). There have been attempts to measure or estimate the microscopic dynamic CA by molecular dynamics (MD) simulation<sup>8–11</sup>, by dynamic density functional theory (DDFT)<sup>12,13</sup> or by a unique combination of precise experiments and theories<sup>14</sup>; however the dependence of the microscopic dynamic CA on the CL velocity, which is essential to develop the boundary condition for the fluid momentum equation with moving CLs, has been little<sup>10,11</sup> explored. Such boundary condition should have an essential importance particularly in hybrid MD/continuum approaches<sup>15,16</sup>, which are now

increasingly feasible.

It is believed that MD simulation is a promising tool to investigate the microscopic physics near moving CLs, but no clear definition of the dynamic CA has been made so far (in e.g.<sup>8–10,17,18</sup>) from the microscopic point of view: fitting the interface to a circular arc to measure CAs is only valid for a droplet under static conditions without gravity<sup>19</sup>. In fact, fitting a different portion of a droplet profile to a circular arc can result in a significant difference in the measured dynamic CA<sup>20</sup>.

In the present study by means of MD simulation, the advancing and receding dynamic CAs (ACA and RCA, respectively) in the vicinity of the CL were obtained by measuring the tangents of the *instantaneous interfaces*<sup>21,22</sup> at a distance of a few adsorption layers (layers in fluid of high density) from the solid surface. A similar attempt has been made recently by Smith *et al.*<sup>11</sup> using a cluster-based interface capturing, but their focus was on the fluctuation in the CAs and much attention was not devoted to the difference between the advancing and receding CAs. An interface-capturing method, called the intrinsic sampling method<sup>23</sup>, was also adopted to elucidate the mechanism of the thermal resistance across a fluid-fluid interface<sup>24</sup> and also to derive an Irving-Kirkwood like formula for the pressure tensor across a liquid-vapour interface that is valid for systems away from equilibrium<sup>25</sup>. As we see later, the present measurement procedure adopting the instantaneous interface method enabled us to extract the structures of the flow and the interface near the moving CLs, which were not smeared by the thermal fluctuations, and to discuss the difference between the advancing and receding CAs.

<sup>a</sup> Department of Mechanical Engineering, Osaka University, 2-1 Yamadaoka, Suita, Osaka 565-0871, Japan. E-mail: t.omori@mech.eng.osaka-u.ac.jp

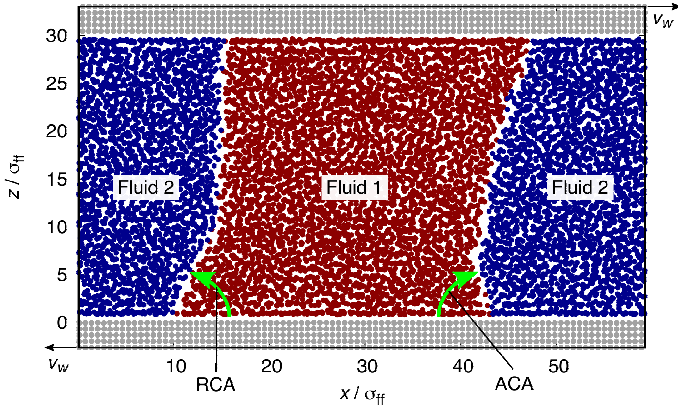


**Fig. 1** Snapshot of the system, a shear flow of two immiscible liquids, where the equilibrium CA  $\theta_e$  and the wall velocity  $v_w$  were  $75^\circ$  and  $0.020\sqrt{\varepsilon_{ff}/m_f}$ , respectively. The positions of the atoms and molecules are projected on a  $xz$  plane. The origin of the  $z$  axis was defined on the innermost (001) plane of the bottom FCC crystal. The length  $L_x$ , the width  $L_y$  and the height  $L_z$  of the channel were  $59.4\sigma_{ff}$ ,  $7.7\sigma_{ff}$  and about  $30.5\sigma_{ff}$ , respectively. The height  $L_z$  varied slightly (1%) under different simulation conditions due to the system pressure control. The temperature control (Langevin thermostat) was applied on the second outermost layers of the wall. The boundaries normal to the wall surface were all periodic.

Based on the unsmoothed fluid density distribution near the CLs, we show that in the definition of the microscopic CA the first adsorption layer must be avoided. This is reminiscent of the observation by Bocquet and Barrat<sup>26</sup> and also by Chen *et al.*<sup>27</sup> in the definition of the hydrodynamic boundary to the solid wall for a single phase fluid. This correspondence has a potential importance in the development of a hydrodynamic boundary condition with moving CLs.

## 2 Problem formulation and methods for simulation

In the present study, two immiscible mono-atomic fluids were confined and sheared by two parallel non-polar solid walls moving at a constant velocity  $v_w$  in opposite directions: a snapshot of the system is shown in Fig. 1. We had 4900 molecules for each fluid and 5520 atoms for the walls. We measured all the CAs, the ACA, RCA and equilibrium CAs from the side of fluid 1. Similarly we call the CLs advancing or receding with respect to fluid 1. For the interaction potential between the fluid molecules and between the solid and fluid molecules, the 12-6 Lennard-Jones (LJ) potential was adopted:

$$\Phi_{LJ}(r_{ij}) = 4\varepsilon_{\alpha\beta} \left[ \left( \frac{\sigma_{\alpha\beta}}{r_{ij}} \right)^{12} - \delta_{\alpha\beta} \left( \frac{\sigma_{\alpha\beta}}{r_{ij}} \right)^6 \right], \quad (1)$$

where  $r_{ij}$  is the distance between molecules  $i$  and  $j$ . We set the parameters (Tab. 1) so that we investigated the two cases with respect to the equilibrium CA  $\theta_e$ , namely  $\theta_e = 90^\circ$ ,  $75^\circ$ . In the present study, a quadratic function was added to the RHS of eqn (1) so that  $\Phi_{LJ}(r_{ij})$  and  $\Phi'_{LJ}(r_{ij})$  smoothly vanished at the cut-off distance  $r_{ij} = 2.5\sigma_{\alpha\beta}$ . The equations of motion were integrated by means of the velocity Verlet algorithm with a time step of  $2.69 \times 10^{-3} \sqrt{m_f \sigma_{ff}^2 / \varepsilon_{ff}}$ . Each solid wall consisted of 5 layers of atoms in the (001) plane of a FCC crystal with a lattice con-

$(\alpha, \beta)$		$\sigma_{\alpha\beta}$ [Å]	$\varepsilon_{\alpha\beta}$ [J]	$\delta_{\alpha\beta}$ [-]
$(f_I, f_J)$	if $I = J$	3.40	$1.67 \times 10^{-21}$	1
	if $I \neq J$	3.40	$1.67 \times 10^{-21}$	-1
$(f_1, s)$	if $\theta_e = 90^\circ$	$1.04 \sigma_{f_1 f_1}$	$1.16 \varepsilon_{f_1 f_1}$	1
	if $\theta_e = 75^\circ$	$1.04 \sigma_{f_1 f_1}$	$1.16 \varepsilon_{f_1 f_1}$	1
$(f_2, s)$	if $\theta_e = 90^\circ$	$1.04 \sigma_{f_2 f_2}$	$1.16 \varepsilon_{f_2 f_2}$	1
	if $\theta_e = 75^\circ$	$1.04 \sigma_{f_2 f_2}$	$0.928 \varepsilon_{f_2 f_2}$	1

**Table 1** Parameters in the LJ potential. The letters “f” and “s” represent fluid and solid, respectively, and the subscripts to “f” take either 1 or 2 to denote the fluid type. These subscripts may be omitted in the case without ambiguity. Fluids of the two different types are immiscible to each other with  $\delta = -1$ <sup>7,18,28</sup>. According to Thompson and Robbins<sup>18</sup>, the CA behaviour is not affected by the value of  $\delta$  when  $-1 \leq \delta \leq 0$ . The angle  $\theta_e$  denotes the equilibrium CA measured from the side of fluid 1.

stant of  $0.91\sqrt{2}\sigma_{ff}$ ; therefore, the wall surface was atomistically smooth. The interaction between the wall atoms was described by the harmonic potential between the nearest neighbors

$$\Phi_H(r_{ij}) = k(r_{ij} - r_0)^2/2 \quad (2)$$

with  $k = 3.24 \times 10^3 \varepsilon_{ff} / \sigma_{ff}^2$  and  $r_0 = 0.91\sigma_{ff}$ . The sheared flows were generated by moving the outermost layers of the solid walls at constant speeds and the temperature of the system was controlled at  $1.10\varepsilon_{ff}/k_B$  by applying the Langevin thermostat<sup>29</sup> on the layers next to the shear generating layers. The thermostatting layer was placed far enough from the liquid so that the thermostatted wall atoms did not directly interact with the liquid molecules. We limited the temperature control to the atom velocities in the  $x - y$  plane to avoid the fluctuation in the system pressure as a possible side-effect. The system temperature remained within  $0.06\varepsilon_{ff}/k_B$  of the target temperature throughout the simulations. The magnitude of the velocity gradient observed in the present study was no more than  $0.03\sqrt{\varepsilon_{ff}/m_f\sigma_{ff}^2}$ , for which one expects<sup>30</sup> the flow to be in the linear response regime. The height of the channel was determined so that the system pressure was  $1.65\varepsilon_{ff}/\sigma_{ff}^3$ : the top wall (moving with a constant velocity in  $x$  direction) was considered as a piston in  $z$  direction<sup>31,32</sup>, where for the first  $t_r \equiv 2.69 \times 10^3 \sqrt{m_f \sigma_{ff}^2 / \varepsilon_{ff}}$  period the initial equilibration was performed; for the second  $t_r$  period the time-averaged  $z$  position of the top wall ( $\bar{z}^{top}$ ) was calculated; for the last  $t_r$  period the final equilibration was conducted with the  $z$  position of the top wall fixed at  $\bar{z}^{top}$ .

The CA and the CL velocity were measured from a level set of the coarse-grained density field<sup>22</sup> defined as

$$\bar{\rho}_1(\mathbf{r}) = \sum_{i \in f_1} \phi(|\mathbf{r} - \mathbf{r}_i|) \quad (3)$$

with

$$\phi(r) = \exp(-r^2/2\xi^2)/2\pi\xi^2, \quad (4)$$

where  $\mathbf{r}_i$  is the coordinate of fluid molecule  $i$  of type  $I$  ( $I = 1, 2$ ) in the  $xz$  plane considering the two-dimensionality of the present system. The instantaneous interface profile was obtained by finding  $\mathbf{r}$  that satisfied  $\bar{\rho}_1(\mathbf{r}) = \bar{\rho}_2(\mathbf{r})$ . We employed  $\xi = 0.28\sigma_{ff}$ , which is smaller than the value adopted by Ravipati *et al.*<sup>33</sup> to analyze

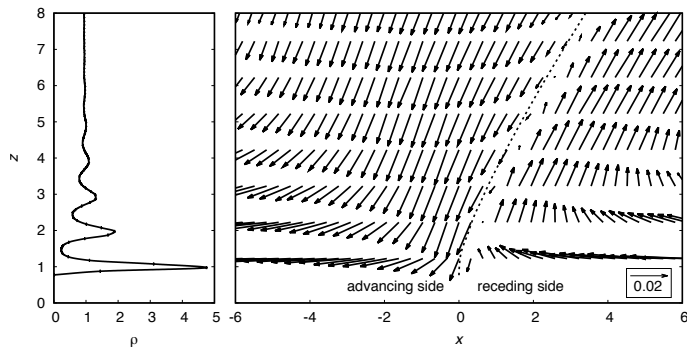


**Fig. 2** (Left) Density distribution  $\rho$  of the fluid near the wall surface measured in a region away from the fluid-fluid interfaces ( $\theta_e = 90^\circ$ ). (Right) Velocity distribution near the CL formed on the bottom wall that was moving in the  $-x$  direction ( $\theta_e = 90^\circ$ ). The dotted line denotes the interface profile.

the equilibrium CA of a sessile droplet: we made  $\xi$  as small as possible to resolve the layer structure of the fluid (the so-called adsorption layers) formed near the walls but large enough so that the interface was captured throughout the simulations. The position of the instantaneous CL was obtained as the intersection of the instantaneous interface profile and  $z = 0$ . The equilibrium position of the innermost layer of the bottom wall was defined as  $z = 0$  (see Fig. 1). The instantaneous density and velocity distributions with its origin at the instantaneous CL were collected to calculate their time-averages.

To estimate the statistical uncertainty in time-averaged quantities, 200 independent simulations with different random number series in the Langevin thermostat were conducted. For all the results in the present study (the left panels of Figs. 2 and 3, Fig. 4 and Fig. 5) the uncertainty is shown with error bars, which represent the 95% confidence interval of each average. Each simulation was conducted for  $3.77 \times 10^3 \sqrt{m_f \sigma_{ff}^2 / \epsilon_{ff}}$  in time, over which the time averages were calculated, after the system was equilibrated and reached a steady state. We determined that the system was in a steady state by seeing the CL not show a systematic drift. The two fluids were in the liquid state and there was no formation of vapor during the simulations. In the following, all physical quantities are non-dimensionalized by  $m_f$ ,  $\sigma_{ff}$  and  $\epsilon_{ff}$  and these bases for the reduced units are not shown for the sake of brevity.

## 3 Results and discussions

### 3.1 Flow field and the definition of the microscopic CA

Figure 2 shows the time-averaged density and velocity distributions of the fluids near the moving wall for  $\theta_e = 90^\circ$ . The left panel of the figure shows the density distribution of the fluids away from the fluid-fluid interfaces, where the existence of the adsorption layers were exhibited. The location of the adsorption layers was identical for  $\theta_e = 90^\circ$  and  $75^\circ$  because of the identical  $\sigma_{fs}$  in the present study. Shown in the right panel of the figure is the velocity distribution near the moving CL for  $\theta_e = 90^\circ$ . The velocity distribution for  $\theta_e = 75^\circ$  was qualitatively the same. By virtue of the instantaneous interface method, a continuous ve-

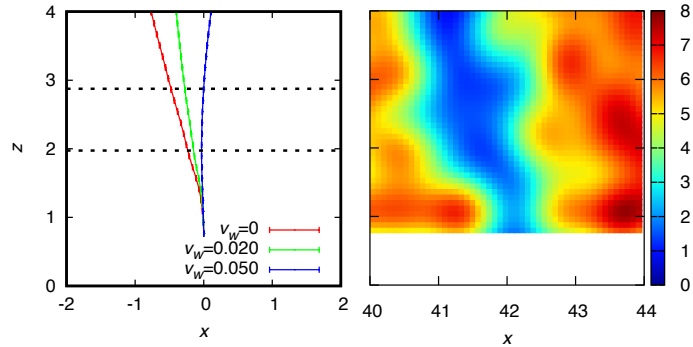


**Fig. 3** (Left) Time-averaged interface profiles under different wall velocities  $v_w$  near the advancing CL ( $\theta_e = 75^\circ$ ). The bottom wall was moving in the  $-x$  direction. The dotted lines denote the positions of the second ( $z = 2.0$ ) and the third ( $z = 2.9$ ) adsorption layers. (Right) Instantaneous coarse-grained density profile,  $\bar{\rho}_1 + \bar{\rho}_2$  (eqn 3), near the CL under  $v_w = 0$  ( $\theta_e = 75^\circ$ ).

locity field, which had a corner-flow like structure, was extracted with a high spacial resolution. We can observe that there is a maximum slip velocity on the CL, which should regularize the stress singularity on the CL.

The left panel of Fig. 3 shows the time-averaged interface profiles near the advancing CL for  $\theta_e = 75^\circ$  under different wall velocities. The interface around  $z = 1$  was perpendicular to the wall surface regardless of the wall velocity even if  $\theta_e \neq 90^\circ$ . The right panel of Fig. 3 shows an instantaneous coarse-grained density distribution of the fluids,  $\bar{\rho}_1 + \bar{\rho}_2$  (eqn 3), near the same CL as in the left panel ( $\theta_e = 75^\circ$ ) under the static condition. As we can see from the figure, there was always an isolated density contour around the first adsorption layer ( $z = 1.0$ ), where no meaningful interface profile regarding the CL dynamics can be extracted\*. We therefore calculated the microscopic CAs as the linear-interpolation of the interface profiles between the second and the third adsorption layers as the nearest possible measurement location from the solid wall; the equilibrium CAs were measured in the same way.

### 3.2 Dynamics of the microscopic CA

Shown in Fig. 4 is the dependence of the microscopic CA on the CL velocity  $v_{CL}$  for two systems with different equilibrium CAs  $\theta_e = 90^\circ$  and  $75^\circ$  respectively, where the microscopic CA  $\theta_w$  was shown in the form  $\cos \theta_e - \cos \theta_w$ , a non-dimensionalized uncompensated Young stress<sup>1</sup>, as a function of the capillary number  $Ca$  defined as  $\eta v_{CL} / \gamma$ , where  $\eta$  is the bulk fluid viscosity and  $\gamma$  is the interfacial tension between the two fluids. We measured  $\eta$  and  $\gamma$  in independent simulations under the identical temperature and pressure as the present study:  $\eta = 1.52$  as the ratio between the shear stress and the bulk velocity gradient in the same system as the present study but without the fluid-fluid interface;  $\gamma = 2.32$  by

\* This is not any artifact of the simulation method adopted in the present study. The liquid has the highest density in the first adsorption layer, which is a mono-molecular layer, and the lowest density between the first and second adsorption layers. This contrast makes the density contour around the first adsorption layer isolated when it is measured with a sufficiently high spacial resolution.

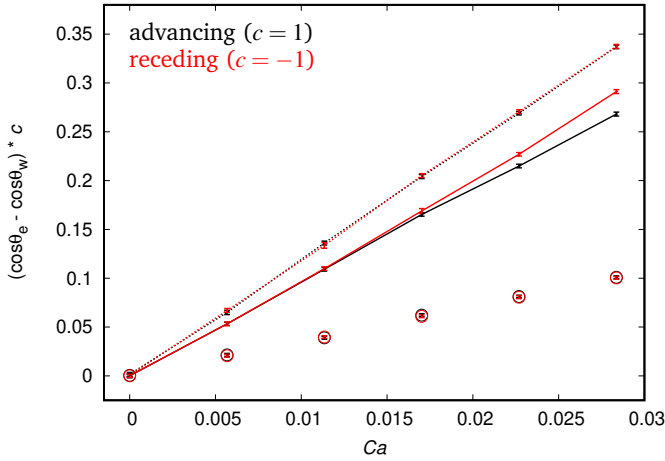


**Fig. 4** Dependence of the advancing and receding microscopic dynamic CAs  $\theta_w$  on the CL velocity  $v_{\text{CL}}$ . The CL velocity is shown as  $Ca = \eta v_{\text{CL}}/\gamma$ , where  $\eta$  is the fluid viscosity and  $\gamma$  is the interfacial tension between the two fluids. The error bar for the abscissa is not shown because  $v_{\text{CL}}$  should be considered given in the steady state simulation: any uncertainty in the determination of  $Ca$  only stretches the figure in the horizontal direction and does not affect the conclusion of the present study. The factor  $c$  (either 1 or  $-1$ ) is to make the comparison between the ACA and the RCA easier. The broken lines are for  $\theta_e = 90^\circ$  with  $\varepsilon_{f1s} = \varepsilon_{f2s} = 1.16$  and solid lines for  $\theta_e = 75^\circ$  with  $\varepsilon_{f1s} = 1.16$  and  $\varepsilon_{f2s} = 0.928$ . The symbols show the results for the system where the two solid-fluid interaction parameters were equally halved from  $\varepsilon_{f1s} = \varepsilon_{f2s} = 1.16$  to  $\varepsilon_{f1s} = \varepsilon_{f2s} = 0.58$  and thus  $\theta_e$  remained  $90^\circ$ .

applying the Bakker equation<sup>34,35</sup> to the fluid-fluid interface in an equilibrium system. No hysteresis was observed on the atomistically smooth surface investigated in the present study. The figure indicates that the uncompensated Young stress has a linear dependence on the CL velocity regardless of  $\theta_e$  as recently reported in the literature<sup>10</sup>. What deserves attention is that a slight difference was observed between the ACA and the RCA for  $\theta_e = 75^\circ$  while they were identical for  $\theta_e = 90^\circ$ .

There are a number of models that relate the dynamic CA to the CL velocity, such as the model by Kistler<sup>36</sup> based on the experimental data by Hoffman<sup>37</sup>, the Hoffman-Voinov-Tanner law<sup>36,38</sup>, the pure hydrodynamic models<sup>39,40</sup> and the molecular kinetic theory (MKT)<sup>41</sup> to mention a few. In principle, only the MKT describes the *microscopic* dynamic CA. The MKT formula written<sup>42</sup> as  $\cos \theta_e - \cos \theta_w = \alpha \exp[\gamma(1 + \cos \theta_e)/(k_B T)] Ca \propto Ca$ , where  $\gamma$  is the fluid interfacial tension,  $T$  is the temperature, and  $\alpha$  is a constant that depends on the fluid molecule size and the solid lattice constant, does not capture the observed difference between the ACA and the RCA. Note that this formula is describing one-fluid systems in the small  $Ca$  regime and it is fair to say that the theory is under development for two-fluid systems<sup>8,20</sup>.

To investigate the reason for the different behaviours of dynamic CA under different equilibrium CAs observed in Fig. 4, we measured the density distribution of the fluids near the CL in the first adsorption layer. It should reveal the mechanical interaction between the solid wall and the fluids because the first adsorption layer is responsible for the friction between the solid wall and the fluids: the friction force is the summation of the tangential force

between each solid atom and fluid molecule and it has been reported that this summation almost saturates to the total friction force in the first adsorption layer<sup>7,43–45</sup>. Figure 5 shows such distribution on the bottom wall near the advancing and receding CLs for two systems with different equilibrium CAs  $\theta_e = 90^\circ$  and  $75^\circ$  respectively. The density on the advancing side decreased and the density on the receding side slightly increased in both systems by increasing the wall velocity. It was due to the corner flow where the pressure is decreased on the advancing side and increased on the receding side<sup>6</sup>. Note that we have observed the height of the first adsorption layer remained the same although its fluid density was affected by the flow.

The asymmetric change of fluid density in the first adsorption layer with respect to the CL resulted in the difference between the solid-fluid friction around the advancing and receding CLs when  $\theta_e = 75^\circ$ . For  $\theta_e = 75^\circ$ , the affinity of the wall to the fluid molecules on the two sides of the CL were different and the integrated friction around the CLs was larger for the receding CL than for the advancing CL (the CLs are called advancing or receding with respect to fluid 1 as we defined at the beginning of section 2). When  $\theta_e = 90^\circ$ , the fluid molecules on both sides of the CL had the identical affinity to the wall and therefore the asymmetric density change near the CL did not cause difference in the solid-fluid friction between the advancing and receding CLs.

How does the solid-fluid friction affect the dynamic CA? This is what we want to address now. At the solid-fluid boundary near the CL without hysteresis, the solid-fluid friction force on the solid side is equal to the summation of the capillary and the viscous forces on the fluid side. If we consider the capillary force is equal to the integration of the uncompensated Young stress across the CL<sup>7</sup>, the mechanical balance at the solid-fluid boundary is written<sup>6</sup> as

$$\int_{\text{int}} \left( \frac{u_t^{\text{slip}}}{l} - \frac{\partial u_t}{\partial x_n} \right) dx_t = \frac{v_{\text{CL}}}{Ca} (\cos \theta_e - \cos \theta_w), \quad (5)$$

where the subscripts  $t$  and  $n$  denote tangential and normal to the wall surface respectively and the variables are shown in non-dimensionalized forms. The shear rate of the flow on the boundary is written as  $\partial u_t / \partial x_n$ ,  $v_{\text{CL}}$  is the CL velocity relative to the wall,  $u_t^{\text{slip}}$  is the fluid slip velocity and  $l$  is the slip length that is inversely proportional to the solid-fluid friction coefficient. The friction coefficient is the friction force per unit wall surface area divided by the fluid slip velocity and larger for the solid-fluid pair with stronger affinity. Because the LHS of eqn (5) and the CL velocity  $v_{\text{CL}}$  on the RHS approximately scale with the slip velocity  $u_t^{\text{slip}}$  on the CL, there is a linear relationship  $\cos \theta_e - \cos \theta_w \propto Ca$  as we have observed in Fig. 4. We measured the second term on the LHS of eqn (5) and the RHS of eqn (5), and the former was one order of magnitude smaller than the latter in the systems investigated (e.g., for  $Ca = 0.028, 0.033$  against  $0.52$  for  $\theta_e = 90^\circ$  and  $0.028$  against  $0.45$  (RCA) and  $0.033$  against  $0.41$  (ACA) for  $\theta_e = 75^\circ$ ). Noting that eqn (5) is a general expression except a possible modification in the definition of  $\theta_e$  discussed at the end of this section, we conclude that the proportionality constant  $(\cos \theta_e - \cos \theta_w)/Ca$  was mainly controlled by the slip length near



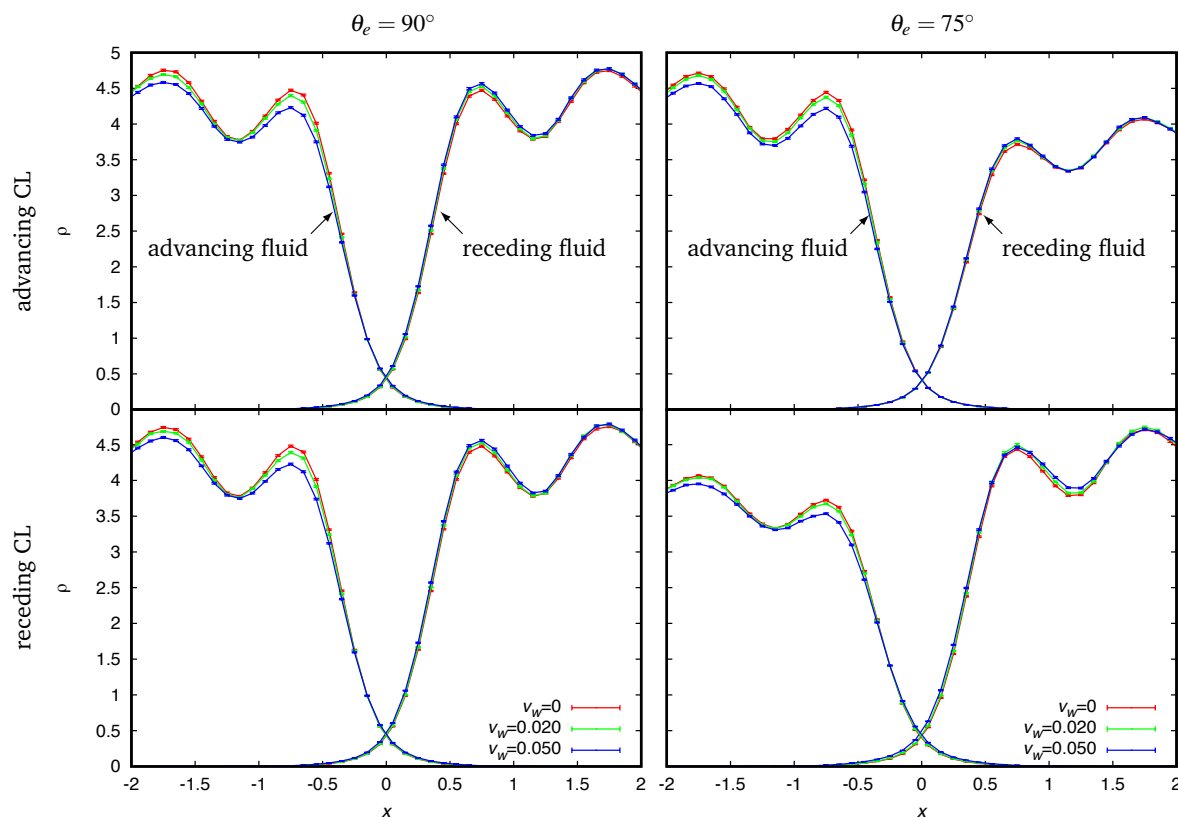


**Fig. 5** Influence of the wall velocity on the density distribution of the two fluids in the first adsorption layer near the advancing and receding CLs. The CLs are called advancing or receding with respect to fluid 1 as we defined at the beginning of section 2. The corner flows near the CL caused asymmetric changes in the density distribution with respect to the CLs.

the CL and therefore, it was larger for the RCA than for the ACA under  $\theta_e = 75^\circ$ . The globally larger proportionality constant for  $\theta_e = 90^\circ$  than for  $\theta_e = 75^\circ$  can be similarly explained.

The importance of considering the solid-fluid friction in the prediction of the dynamic CA is further evident when we observe the results under different solid-fluid interaction parameters. Figure 4 also compares the behaviours of the microscopic dynamic CA under the halved solid-fluid interaction parameters ( $\varepsilon_{f1s} = \varepsilon_{f2s} = 0.58$ , shown with symbols) and under the original parameters ( $\varepsilon_{f1s} = \varepsilon_{f2s} = 1.16$ ) for  $\theta_e = 90^\circ$ . This result illustrated that even under the same equilibrium CA the dynamic CAs were different when the solid-fluid friction coefficients were different.

Remarks should be made here about the assumption to derive eqn (5). In the derivation, it was assumed that the capillary force near the moving CL can be described by the uncompensated Young stress. This assumption, however, is probably not true. Considering the density change in the first adsorption layer induced by the flow that we have seen in Fig. 5, the equilibrium contribution in the capillary force may deviate<sup>19</sup> from  $\cos \theta_e$ . How this deviation can affect the seemingly linear relationship  $\cos \theta_e - \cos \theta_w \propto Ca$  should be addressed in future works.

## 4 Concluding remarks

By means of molecular dynamics simulation, we have analyzed the advancing and receding microscopic contact angles formed by two immiscible mono-atomic fluids and a non-polar solid wall. In the definition of the microscopic contact angle, the first adsorption layer on the wall was excluded based on the high-resolution

density profile of the fluids near the contact line obtained by the instantaneous interface method. The contact angle was measured by the local interface tangent without resorting to circular-arc fitting of the moving fluid-fluid interface.

We demonstrated that the uncompensated Young stress was proportional to the capillary number under the whole range of the capillary number up to 0.03. We have found the difference in the constant of proportionality between the advancing and receding contact angles when the equilibrium contact angle is not 90 degrees and this difference can be attributed to the asymmetric density change near the moving contact line induced by the corner flow. We hope that the present results provide useful information also to be integrated into the existing state-of-the-art dynamic contact angle models.

To conclude, we would like to address the practical aspect of the findings of the present study. Writing the advancing and receding contact angles as  $\theta_{w,a}$  and  $\theta_{w,r}$  respectively, the total capillary force imposed on the flow is  $2\gamma(\cos \theta_{w,a} - \cos \theta_{w,r})$  per unit channel width if we neglect the possible variation of the equilibrium contribution due to the flow. The total capillary force can then be expressed as  $2\gamma(\cos \theta_{w,a} - \cos \theta_{w,r}) = -2(\alpha_a + \alpha_r)Ca$ , where the coefficients  $\alpha_a$  and  $\alpha_r$  are the slopes in Fig. 4 for the advancing and receding contact angles, respectively. It means that more resistance was induced around the receding contact line than around the advancing contact line in systems with  $\theta_e < 90^\circ$ . This phenomenon should have impact on the industrial applications of the two-component or two-phase fluid transportation in

fine pores. For two-phase flows with contact lines, the fluid density in the first adsorption layer is different between each side of the contact line and the advancing and receding contact angles will show the asymmetrical behaviour as observed for  $\theta_e < 90^\circ$  in the present study.

## Conflicts of interest

There are no conflicts to declare.

## Acknowledgements

This work was financially supported by JSPS KAKENHI Grant Nos. 15K17974, 18K03929 and 18K03978. YY was also supported by JST CREST Grant No. JPMJCR1811, Japan. The authors thank Laurent Joly of Université Lyon 1 for fruitful discussions.

## References

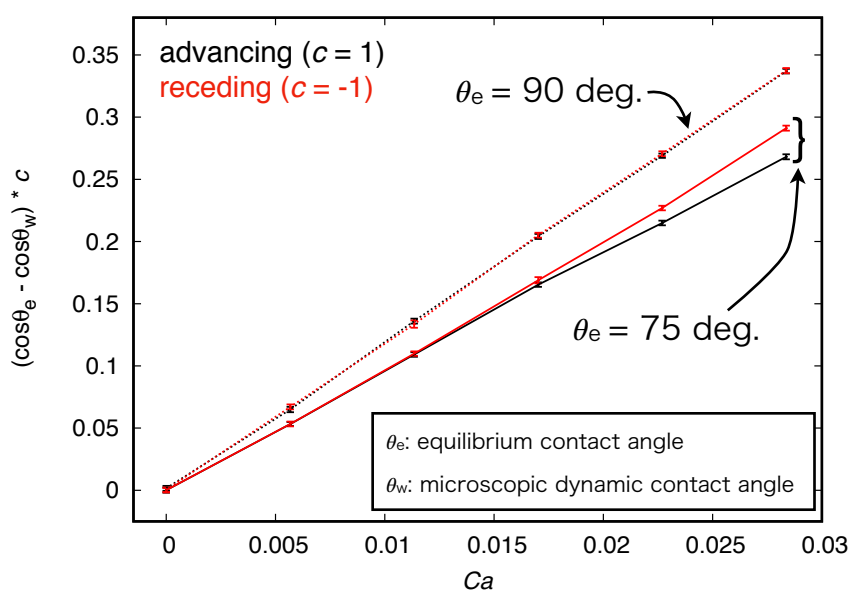
- 1 D. Bonn, J. Eggers, J. Indekeu and J. Meunier, *Reviews of Modern Physics*, 2009, **81**, 739–805.
- 2 J. H. Snoeijer and B. Andreotti, *Annual Review of Fluid Mechanics*, 2013, **45**, 269–292.
- 3 N. G. Hadjiconstantinou, *Physical Review E*, 1999, **59**, 2475–2478.
- 4 E. Ramé, S. Garoff and K. R. Willson, *Physical Review E*, 2004, **70**, 031608.
- 5 J. H. Snoeijer, *Physics of Fluids*, 2006, **18**, 021701.
- 6 T. Omori and T. Kajishima, *Physics of Fluids*, 2017, **29**, 112107.
- 7 T. Qian, X.-P. Wang and P. Sheng, *Physical Review E*, 2003, **68**, 016306.
- 8 D. Seveno, T. D. Blake, S. Goossens and J. De Coninck, *Langmuir*, 2011, **27**, 14958–14967.
- 9 A. Malani, A. Raghavanpillai, E. B. Wysong and G. C. Rutledge, *Physical Review Letters*, 2012, **109**, 184501.
- 10 T. D. Blake, J.-C. Fernandez-Toledano, G. Doyen and J. De Coninck, *Physics of Fluids*, 2015, **27**, 112101.
- 11 E. R. Smith, E. A. Müller, R. V. Craster and O. K. Matar, *Soft Matter*, 2016, **12**, 9604–9615.
- 12 B. D. Goddard, A. Nold, N. Savva, P. Yatsyshin and S. Kalliadasis, *Journal of Physics: Condensed Matter*, 2013, **25**, 035101.
- 13 A. Nold, *PhD thesis*, Imperial College London, 2016.
- 14 R. Lhermerout, H. Perrin, E. Rolley, B. Andreotti and K. Davitt, *Nature Communications*, 2016, **7**, 12545.
- 15 N. G. Hadjiconstantinou, *Journal of Computational Physics*, 1999, **265**, 245–265.
- 16 J. Zhang, M. K. Borg and J. M. Reese, *International Journal of Heat and Mass Transfer*, 2017, **115**, 886–896.
- 17 J. Koplik, J. R. Banavar and J. F. Willemsen, *Physical Review Letters*, 1988, **60**, 1282–1285.
- 18 P. A. Thompson and M. O. Robbins, *Physical Review Letters*, 1989, **63**, 766–769.
- 19 Y. Yamaguchi, H. Kusudo, D. Surbly, T. Omori and G. Kikugawa, *The Journal of Chemical Physics*, 2019, **150**, 044701.
- 20 D. Seveno, T. D. Blake, S. Goossens and J. De Coninck, *Langmuir*, 2018, **34**, 5160–5161.
- 21 G. Kikugawa, S. Takagi and Y. Matsumoto, *Computers and Fluids*, 2007, **36**, 69–76.
- 22 A. P. Willard and D. Chandler, *The Journal of Physical Chemistry B*, 2010, **114**, 1954–1958.
- 23 E. Chacón and P. Tarazona, *Physical Review Letters*, 2003, **91**, 1–4.
- 24 J. Muscatello, E. Chacón, P. Tarazona and F. Bresme, *Physical Review Letters*, 2017, **119**, 1–5.
- 25 C. Braga, E. R. Smith, A. Nold, D. N. Sibley and S. Kalliadasis, *The Journal of Chemical Physics*, 2018, **149**, 044705.
- 26 L. Bocquet and J.-l. Barrat, *Physical Review E*, 1994, **49**, 3079–3092.
- 27 S. Chen, H. Wang, T. Qian and P. Sheng, *Physical Review E*, 2015, **92**, 043007.
- 28 W. Ren and W. E, *Physics of Fluids*, 2007, **19**, 022101.
- 29 J. Blömer and A. Beylich, *Surface Science*, 1999, **423**, 127–133.
- 30 P. A. Thompson and S. M. Troian, *Nature*, 1997, **389**, 360–362.
- 31 S. Nakaoka, Y. Yamaguchi, T. Omori, M. Kagawa, T. Nakajima and H. Fujimura, *Physical Review E*, 2015, **92**, 022402.
- 32 S. Nakaoka, Y. Yamaguchi, T. Omori and L. Joly, *The Journal of Chemical Physics*, 2017, **146**, 174702.
- 33 S. Ravipati, B. Aymard, S. Kalliadasis and A. Galindo, *The Journal of Chemical Physics*, 2018, **148**, 164704.
- 34 G. Bakker, *Kapillarität und Oberflächenspannung*, Akademische Verlagsgesellschaft, 1928.
- 35 S. Ono and S. Kondo, *Structure of Liquids*, Springer, 1960, pp. 134–280.
- 36 S. F. Kistler, *Wettability*, Taylor & Francis, 1993, ch. 6, pp. 311–429.
- 37 R. L. Hoffman, *Journal of Colloid and Interface Science*, 1975, **50**, 228–241.
- 38 L. H. Tanner, *Journal of Physics D: Applied Physics*, 1979, **12**, 1473–1484.
- 39 R. G. Cox, *Journal of Fluid Mechanics*, 1986, **168**, 169–194.
- 40 R. Cox, *Journal of Fluid Mechanics*, 1998, **357**, 249–278.
- 41 T. Blake and J. Haynes, *Journal of Colloid and Interface Science*, 1969, **30**, 421–423.
- 42 T. Blake and J. De Coninck, *Advances in Colloid and Interface Science*, 2002, **96**, 21–36.
- 43 Y. Hizumi, T. Omori, Y. Yamaguchi and T. Kajishima, *Transactions of the JSME (in Japanese)*, 2015, **81**, 15–00409.
- 44 S. K. Bhatia and D. Nicholson, *Langmuir*, 2013, **29**, 14519–14526.
- 45 K. Falk, F. Sedlmeier, L. Joly, R. R. Netz and L. Bocquet, *Langmuir*, 2012, **28**, 14261–14272.

## Table of contents entry

for

# Understanding the asymmetry between the advancing and receding microscopic contact angles

T. Omori, Y. Kobayashi, Y. Yamaguchi and T. Kajishima



Our molecular dynamics simulation has revealed the asymmetric behaviour between the advancing and receding contact angles even on smooth surfaces.